Locally Concentrated Ionic Liquid Electrolyte with Partially Solvating Diluent for Lithium/Sulfurized Polyacrylonitrile Batteries

Xu Liu, Thomas Diemant, Alessandro Mariani, Xu Dong, Maria Enrica Di Pietro, Andrea Mele, and Stefano Passerini*

The development of Li/sulfurized polyacrylonitrile (SPAN) batteries requires electrolytes that can form stable electrolyte/electrode interphases simultaneously on lithium-metal anodes (LMAs) and SPAN cathodes. Herein, a low-flammability locally concentrated ionic liquid electrolyte (LCILE) employing monofluorobenzene (mFBn) as the diluent is proposed for Li/SPAN cells. Unlike non-solvating diluents in other LCILEs, mFBn partially solvates Li⁺, decreasing the coordination between Li⁺ and bis(fluorosulfonyl)imide (FSI⁻). In turn, this triggers a more substantial decomposition of FSI⁻ and consequently results in the formation of a solid electrolyte interphase (SEI) rich in inorganic compounds, which enables a remarkable Coulombic efficiency (99.72%) of LMAs. Meanwhile, a protective cathode electrolyte interphase (CEI), derived mainly from FSI⁻ and organic cations, is generated on the SPAN cathodes, preventing the dissolution of polysulfides. Benefiting from the robust interphases simultaneously formed on both the electrodes, a highly stable cycling of Li/SPAN cells for 250 cycles with a capacity retention of 71% is achieved employing the LCILE and only 80% lithium-metal excess.

1. Introduction

Sulfur, due to its high specific capacity (1675 mAh g⁻¹) and low cost, is a promising cathode material for high-energy-density rechargeable lithium-metal batteries (LMBs), i.e., lithium–

X. Liu, T. Diemant, A. Mariani, X. Dong, S. Passerini
Helmholtz Institute Ulm (HIU)
Helmholtzstraße 11, D-89081 Ulm, Germany
E-mail: stefano.passerini@kit.edu
X. Liu, T. Diemant, A. Mariani, X. Dong, S. Passerini
Karlsruhe Institute of Technology (KIT)
P.O. Box 3640, D-76021 Karlsruhe, Germany
M. E. Di Pietro, A. Mele
Department of Chemistry, Materials and Chemical Engineering
"Giulio Natta"
Politecnico di Milano
Piazza Leonardo da Vinci 32, Milan I-20133, Italy

The ORCID identification number(s) for the author(s) of this article can be found under https://doi.org/10.1002/adma.202207155.

sulfur (Li–S) batteries.[1] Nonetheless, the conventional elemental sulfur cathodes with the electrochemical reactions at the host/sulfur/electrolyte three-phase interface suffer from the intrinsic shuttle effect of polysulfides, i.e., the dissolution and migration of polysulfides, which leads to rapid capacity decay and low Coulombic efficiency (CE) of Li–S batteries.[2,3]

In this context, the use of sulfurized polyacrylontrile (SPAN), which shows negligible polysulfide dissolution and stable cycling up to hundreds of cycles due to a solid-phase mechanism in carbonate-based electrolytes, is a valuable alternative path.[4–6] Besides the strong interaction between sulfur fragments and dehydro-cyclized polyacrylontrile skeletons,[7,8] the remarkable electrochemical properties are also closely related to the formation of protective, polycarbonate-based cathode/electrolyte interphases (CEIs) in carbonate-based electrolytes.[9,10] In fact, dissolution of polysulfide and fast capacity decay are still observed when ether-based electrolytes are employed.[9,11] Unfortunately, the conventional carbonate-based electrolytes for commercial lithium-ion batteries are incompatible with lithium-metal anodes (LMAs).[12] The unstable solid-electrolyte interphases (SEIs) result in lithium dendrite growth and low lithium stripping/plating CEs,[13] which further cause safety concerns and limited lifespan of Li/SPAN cells with low negative to positive areal capacity (N/P) ratio.[14,15] Therefore, the development of more practical Li/SPAN cells requires electrolytes that can form stable electrolyte/electrode interphases (EEIs) simultaneously on LMAs and SPAN cathodes.[16–19]

Ionic liquid electrolytes (ILEs) with low flammability and high compatibility toward LMAs are promising candidates for safe and long-lifespan LMBs,[20,21] but their high viscosity and sluggish Li⁺ transport at room temperature limit their further application.[22] Recently, diluting ILEs with non-solvating co-solvents, e.g., hydrofluoroethers or fluorinated aromatic compounds, has been proven to be an effective approach in mitigating the aforementioned deficiencies without compromising the high compatibility toward LMAs,[12,23–25] inspired by organic-solvent-based concentrated electrolytes.[26–30] The co-solvents usually contain highly fluorinated (e.g., trifluoro-, or difluoro-substituted)

groups with strong electron-withdrawing effect weakening the interaction between the co-solvents and the ionic species in ILEs, which allows the dilution of ILEs without affecting the local coordination between Li$^+$ and anions.[12,23–25] The ILEs blended with non-solvating co-solvents are named as locally concentrated ionic liquid electrolytes (LCILEs). To date, a high lithium stripping/plating CE of 99.56% has been recorded with rationally designed LCILEs.[31] With the remarkable compatibility toward LMAs, LCILEs might be promising candidates for Li/SPAN cells. Nonetheless, the electrochemical behavior of SPAN cathodes in ILEs or LCILEs has not been investigated yet. Whether protective CEIs can be formed with these electrolytes allowing stable cycling of SPAN cathodes still remains unknown.

Herein, a new LCILE consisting of lithium bis(fluorosulfonyl) imide (LiFSI), 1-ethyl-3-methylimidazolium bis(fluorosulfonyl) imide (EmimFSI), and monofluorobenzene (mFBn) in a molar ratio of 1:2:2, i.e., [LiFSI]$_1$[EmimFSI]$_2$[mFBn]$_2$ (FEmF) is proposed for Li/SPAN cells. Unlike the non-solvating character of highly fluorinated co-solvents in other LCILEs,[12,24,25] mFBn with relatively lower fluorination partially solvates Li$^+$, decreasing the coordination between Li$^+$ and FSI$^-$. In turn, this triggers a more substantial decomposition of FSI$^-$ and consequently results in the formation of a SEI rich in inorganic compounds, which enables a remarkable lithium stripping/plating CE of 99.72%. This and the high compatibility toward SPAN cathodes in FEmF lead to highly stable cycling of Li/SPAN full cells (80% lithium-metal excess) for up to 250 cycles with a capacity retention of 71%. In contrast, when the mFBn-free neat ILE, i.e., [LiFSI]$_1$[EmimFSI]$_2$ (FE) is employed, the lithium

stripping/plating CE and the Li/SPAN cells' capacity retention are 99.01% and 17%, respectively, under the same conditions. The chemical sketches of the components are shown in Figure S1 (Supporting Information). The compositions of the electrolytes are shown in Table S1 (Supporting Information).

2. Results and Discussion

2.1. Physicochemical Properties and Solvation Structure

Low flammability is one of the most important merits of ILEs for safe LMBs, originating from their high thermal stability and non-volatility. However, mFBn exhibits a flashpoint of −12 °C, i.e., it is highly flammable. Therefore, the flashpoint of the electrolytes was measured to assess their flammability. As expected, no flash was detected for FE in the temperature range of 25–300 °C. In the test of FEmF, a flash occurred at 98 °C, which is associated to the presence of mFBn. According to the American Occupational Safety and Health Standards, any liquid having a flashpoint at or below 93 °C is considered as flammable.[32] The flashpoint of FEmF (98 °C) is higher than the abovementioned threshold value (93 °C); thus it should be considered as a low-flammability electrolyte. Nonetheless, employing diluents with higher flashpoint, stronger ability to capture radical ·H and ·OH, or/and stronger interactions with ionic species in ILs could further decrease the flammability of the electrolyte.[33,34]

The viscosity and ionic conductivity of the electrolytes at various temperatures are shown in **Figure 1**a,b, respectively. The
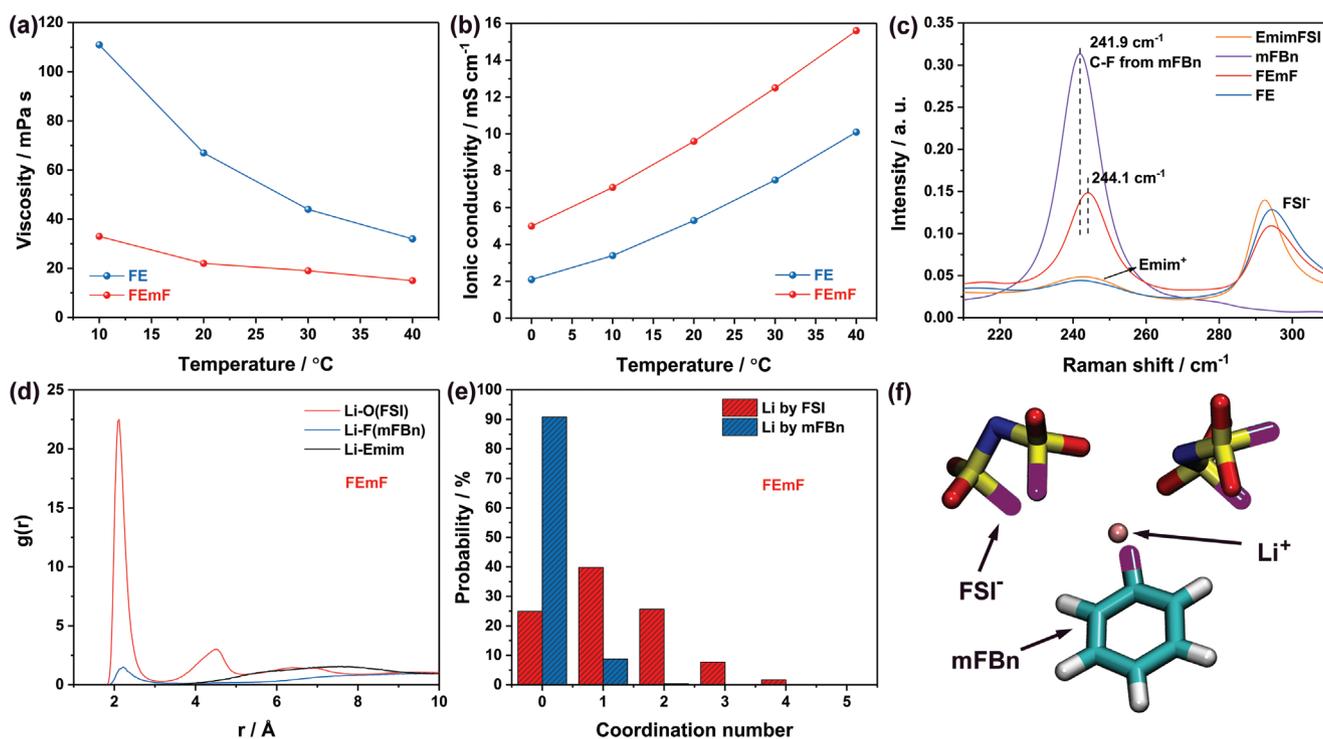

Figure 1. a) Viscosity, and b) ionic conductivity of FE and FEmF. c) Raman spectra of EmimFSI, mFBn, FE, and FEmF in the region relevant to the C–F bond of mFBn. d,e) Results of molecular dynamic simulations of FEmF: d) radial distribution functions of Li–O(FSI), Li–F(mFBn), and Li–Emim pairs; e) coordination number populations of Li by FSI and mFBn; f) a Li$^+$ coordination involving both FSI$^-$ and mFBn.

ADVANCED
SCIENCE NEWS

www.advancedsciencenews.com

ADVANCED
MATERIALS

www.advmat.de

addition of low-viscosity mFBn (0.55 mPa s at 25 °C)[35] to FE effectively decreases the viscosity and increases the ionic conductivity. At 20 °C, the viscosities of FE and FEmF are 68 and 22 mPa s, respectively, while the ionic conductivities of FE and FEmF are 5.3 and 9.6 mS cm^{-1}, respectively. The self-diffusion coefficients of the ions in the electrolytes were examined via pulsed field gradient (PFG) NMR, and the results are shown in Table S2 (Supporting Information). The self-diffusion coefficient of Li$^+$ in FEmF is 3.5×10^{-11} m^2 s^{-1}, which is 2.5 times of that in FE.[31] The apparent Li$^+$ transference number of FEmF was calculated to be 0.118, which is slightly lower than that of FE (0.135). Considering the ionic conductivities and the Li$^+$ transference numbers, one can infer that Li$^+$ transport in FEmF is faster than in FE, which is identical to the higher Li$^+$ self-diffusion coefficient in FEmF.

The solvation structures of Li$^+$ in FE and FEmF were initially characterized via Raman spectroscopy. The coordination state of FSI$^-$ is usually evaluated with the v_s(S–N–S) and v_s(SO$_2$) modes in the region of 700–770 and 1200–1250 cm^{-1}, respectively.[36–38] However, the FSI$^-$ peaks in these regions overlap with peaks originating from Emim$^+$ and/or mFBn (Figure S2, Supporting Information), which hinders further fitting analysis. Nonetheless, the peak mainly representing the aromatic ring of mFBn shifts from 1009.3 cm^{-1} for neat mFBn to 1010.5 cm^{-1} for FEmF (Figure S3, Supporting Information), and the peak originating from the C–F bond of mFBn shifts from 241.9 to 244.1 cm^{-1} (Figure 1c).[39,40] A peak from the CH$_3$–N bending of Emim$^+$ also presents ≈242 cm^{-1},[41] but the comparison to a FSI$^-$ peak ≈294 cm^{-1} indicates that the contribution of the CH$_3$–N peak to the shift of the C–F peak is rather limited. These results demonstrate the involvement of mFBn in the solvation.

To elucidate this effect in more detail, molecular dynamic (MD) simulations of FEmF were conducted. Snapshots are displayed in Figure S4 (Supporting Information). The mFBn-based domains can be distinguished from the network of ionic species, including Li$^+$, FSI$^-$, and Emim$^+$, which corroborates the generally poor solvating ability of mFBn toward ionic species. Nonetheless, the interaction between mFBn and Li$^+$ is evidenced by means of radial distribution functions (RDFs) as shown in Figure 1d. A strong peak at 2.12 Å in the curve of Li–O(FSI) is associated with the dominant coordination of Li$^+$ by FSI$^-$. Despite its lower intensity, an additional peak is clearly seen at 2.22 Å for the Li–F(mFBn) curve, demonstrating the presence of mFBn in the first solvation shell of Li$^+$. The coordination number population of FSI$^-$ and mFBn to Li$^+$ is shown in Figure 1e. The average number of FSI$^-$ and mFBn coordinating each Li$^+$ is calculated to be 1.22 and 0.09, respectively. One Li$^+$ coordination, involving both FSI$^-$ and mFBn, has been extracted from the MD simulation (see Figure 1f) to illustrate the coordination of mFBn to Li$^+$. Nonetheless, it should be noticed that the mFBn-involved coordination is minor, and most of Li$^+$ coordinate only to FSI$^-$ (one such coordination is extracted from the simulation and shown in Figure S5, Supporting Information) as demonstrated in Figure 1e.

The results of Raman spectroscopy and MD simulation demonstrate the partially solvating character of mFBn. In general, the solvation ability of mFBn toward ionic species is poor, which leads to the micro-heterogeneity that is commonly seen for LCILEs. On the other hand, a small portion of mFBn still participates in the solvation of Li$^+$, leading to more "free" FSI$^-$ and fewer coordinated FSI$^-$. The fewer Li$^+$–FSI$^-$ interactions are good for lower viscosity and higher ionic conductivity,[42,43] but lead to concerns with regard to the compatibility of FEmF toward LMAs, as it is widely known that a higher amount of anion coordinating to Li$^+$ helps in the formation of anion-derived inorganic-rich SEIs for a high compatibility toward LMAs.[27,42–44]

2.2. Electrochemical Performance of LMAs

In the next step, the electrochemical performance of LMAs in FE and FEmF was evaluated. The surface morphology of lithium metal (1.5 mAh cm^{-2}) deposited on Cu foil at 0.5 mA cm^{-2} in either FE or FEmF was investigated via scanning electron microscopy (SEM), as displayed in **Figure 2**a,b, respectively. A porous deposition layer consisting of both nodule-like and dendritic lithium is observed for the sample deposited in FE. In contrast, the deposit is only made up of compact nodule-like lithium particles without any dendrite when FEmF is used as the electrolyte. A similar result is also seen from the cross-sectional SEM images (Figure S6, Supporting Information). The elimination of the dendritic growth of lithium helps for the safer operation of the LMBs, while the larger lithium particles can reduce the side reactions at the lithium/electrolyte interface.

The lithium stripping/plating CE in the two electrolytes was measured via cycling of lithium metal deposited on Cu.[28,45] The test protocol can be found in the experimental section while the evolution of cell voltages during the measurements is shown in Figure 2c. The CEs of the initial formation cycle (5.0 mAh cm^{-2}) at 0.5 mA cm^{-2} are 96.35% and 99.00% for FE and FEmF, respectively. In the following 50 cycles (1 mAh cm^{-2} for each cycle) with a plating current density of 0.5 mA cm^{-2} and a stripping current density of 1.5 mA cm^{-2}, the average CE obtained in FE and FEmF are 99.01% and 99.72%, respectively. Therefore, the addition of mFBn to FE effectively reduces the side reactions at the electrolyte/LMA interface, promoting the reversibility of LMAs. Even more important, the remarkable CE of 99.72% is the highest value ever recorded for LCILEs.[12,23–25,31] Therefore, the presence of partially solvating mFBn does not cause negative effects on the compatibility of the electrolyte toward LMAs.

The cyclic stability of LMAs was further assessed via the cycling of symmetric Li/Li cells with a cycling capacity of 1 mAh cm^{-2}. After two formation cycles at 0.1 mA cm^{-2}, a higher current density of 1 mA cm^{-2} was applied for all following cycles. The evolution of the cell voltage is displayed in Figure 2d. In the initial tens of cycles at 1.0 mA cm^{-2}, the Li/FE/Li cell shows polarization of ≈0.2 V, which is higher than that of Li/FE/Cu cells when a stripping current density of 1.5 mA cm^{-2} is applied (Figure 2c). Therefore, the higher polarization of Li/FE/Li cell is mainly related to the LMA interface, i.e., the native SEI of LMAs, rather than the Li$^+$ transport in the electrolyte. In the following cycling, the decreasing voltage implies more and more porous LMAs offering more reaction sites, which, on the other hand, increases the interfacial side reactions. Due to that, a dramatic increase in the voltage is observed after cycling for 1100 h, and
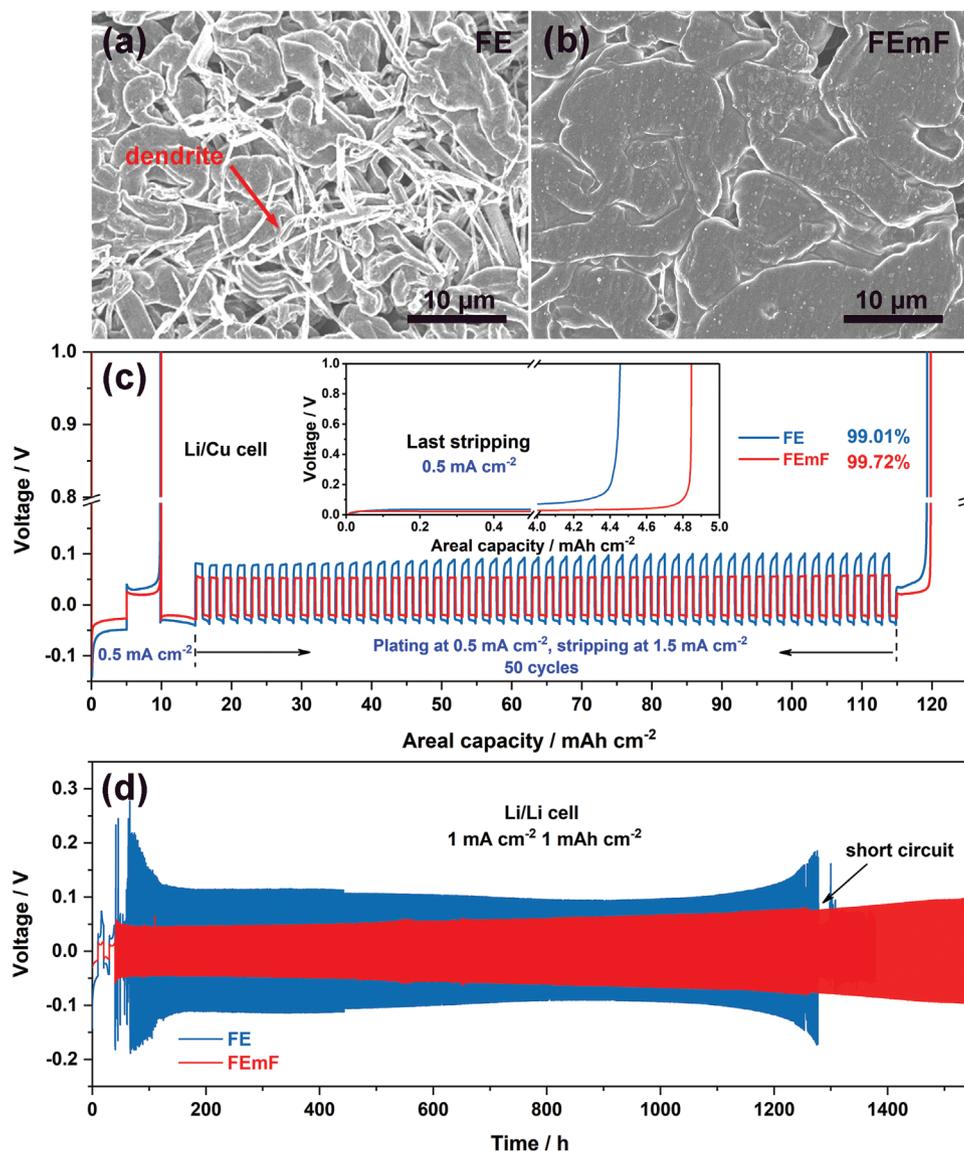
Figure 2. a,b) SEM images illustrating the surface morphology of lithium metal (1.5 mAh cm^{-2}) deposited in FE (a) and FEmF (b) on Cu foil. c) The voltage profile of Li/Cu cells for the evaluation of Li stripping/plating CE in FE and FEmF. The inset shows the voltage profile of the last stripping process. d) Voltage profiles for Li/Li cells employing FE and FEmF upon long-term, galvanostatic stripping/plating cycling.

the cell fails to operate due to a short circuit occurring at 1278 h (621 cycles). In contrast, the cell employing FEmF exhibits a steady operation for more than 1540 h (752 cycles). The average voltage plateau only slightly increases from 39 mV at the 32nd cycle (100 h) to 82 mV at the 752nd cycle (1540 h), as shown in Figure S7 (Supporting Information). These results clearly demonstrate the remarkably promoted compatibility of the electrolyte toward LMAs caused by the addition of mFBn into FE.

2.3. Electrochemical Performance of Li/SPAN Cells

SPAN doped with a small amount of Se was selected as a model compound to investigate the compatibility of the developed electrolytes with Li/SPAN cells, as it has been demonstrated that Se dopant present in the SPAN matrix can promote the

cyclability, and rate capability of SPAN.[8,46–49] The material was prepared via calcination of a mixture of Se, S, and polyacrylonitrile powder with a mass ratio of 1:20:5 at 300 °C for 2 h in an Ar atmosphere.[29,50] The characterization of the SPAN is shown in Figures S8 and S9 (Supporting Information).

As a first step, Li/SPAN coin cells employing thick Li anodes (500 μm, ≈103 mAh cm^{-2}) and excess electrolyte (75 μL) were assembled and cycled in the 1.0-3.0 V voltage window at 20 °C. The average mass loading of SPAN was 2.7 mg cm^{-2}.

After three formation cycles at 0.1C (1C = 500 mA g^{-1} = 1.35 mA cm^{-2}), the cells were cycled at C/3 charge and 1C discharge. The discharge capacities and CEs are shown in **Figure 3**a. The dis-/charge profiles of Li/SPAN cells with FE or FEmF at selected cycles are shown in Figure S10 (Supporting Information) and Figure 3b, respectively. In the initial discharge, 756 and 736 mAh g^{-1} were delivered in FEmF and FE, respectively.
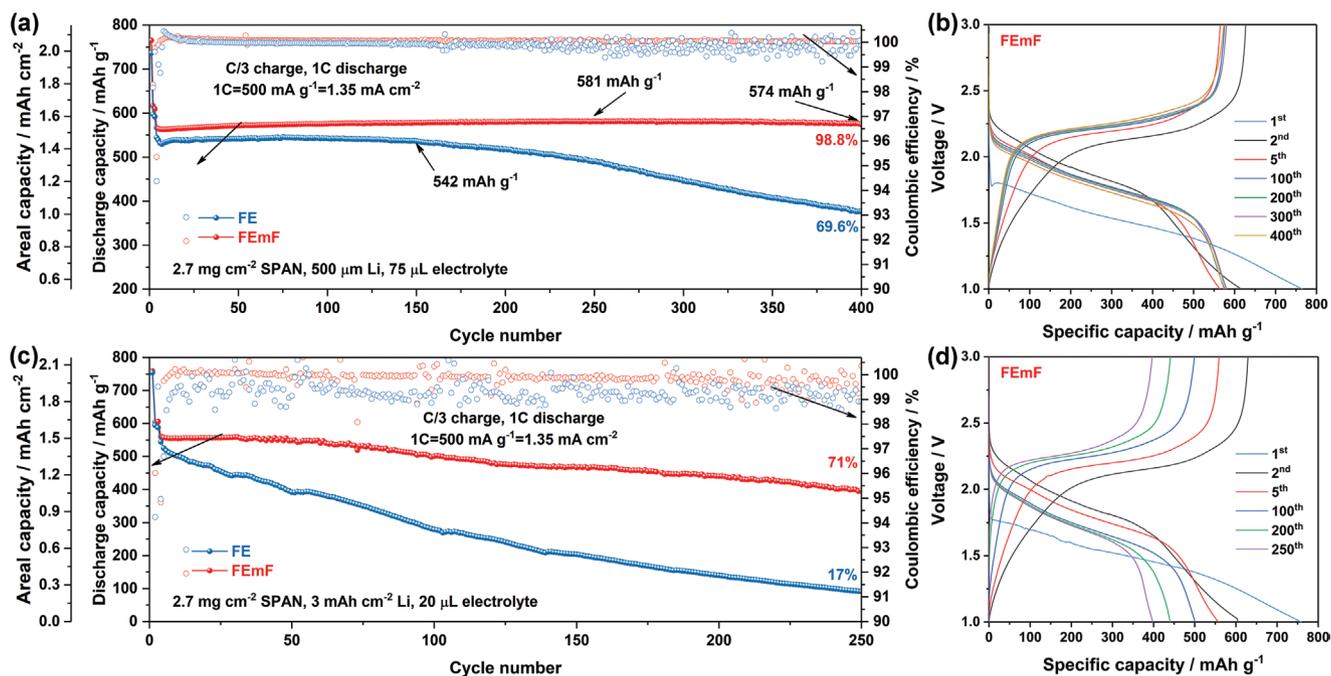
Figure 3. a,b) Electrochemical performance of Li/SPAN cells employing thick LMAs (500 μm, ≈103 mAh cm^{-2}) and excess amount of electrolyte (75 μL): a) evolution of discharge capacity and CE upon cycling at C/3 charge and 1C discharge after three formation cycles at C/10, b) dis-/charge profiles of Li/FEmF/SPAN cells at selected cycles. c,d) Electrochemical performance of Li/SPAN cells employing thin LMAs (3 mAh cm^{-2}) with relatively lean electrolyte (20 μL in each cell): c) evolution of discharge capacity and CE upon cycling at C/3 charge and 1C discharge after three formation cycles at C/10, d) dis-/charge profiles of Li/FEmF/SPAN cells at selected cycles.

In the subsequent cycle, the reversible capacity delivered in FEmF and FE was 616 and 597 mAh g^{-1}, respectively. The capacity difference between the initial two cycles demonstrates that some Li$^+$ cations (≈19% of the initial capacity) are trapped in SPAN upon the initial discharge, being no longer available in the following cycling.[51] At the 5th cycle with elevated current rates, the specific capacities decreased to 539 mAh g^{-1} in FE and 564 mAh g^{-1} in FEmF. The higher specific capacity achieved with FEmF is also observed at different current rates (Figure S11, Supporting Information), demonstrating as this electrolyte offers faster Li$^+$ transport than FE. During the following cycling, the capacity evolution of these two cells is very different. When FE is employed, the specific capacity (≈542 mAh g^{-1}) is very stable in the first 150 cycles with an average CE of 99.9%, implying that a stable CEI preventing the shuttle effect of polysulfides is generated on SPAN. In fact, the poor CEI formed at the interface of SPAN, e.g., in 1 M LiFSI/glyme, results in CEs much lower than 100% and a rapid capacity decay already in the early cycles.[9,11] Nonetheless, the specific capacity of SPAN in FE decreases to 377 mAh g^{-1} at the 400th cycle, corresponding to a capacity retention of 69.6%. This fading can be attributed to the degradation of LMA in FE upon long-term operation (for 1628 h). On the other hand, the cell employing FEmF shows a gradual increase of specific capacity to 581 mAh g^{-1} at the 250th cycle, finally reaching 574 mAh g^{-1} at the 400th cycle (1909 h), which corresponds to a capacity retention of 98.8%. This remarkable cyclability originates not only from the durable LMA in FEmF, but also from the excellent CEI and interfacial stability of SPAN.

In a further step, SPAN cathodes (2.7 mg cm^{-2}) and thin LMAs (areal capacity of 3 mAh cm^{-2}) were coupled in cells, exhibiting an N/P ratio of 1.8. Since SPAN does not contain Li$^+$, the N/P ratio of the cell corresponds to a low Li excess, i.e., 80%. Meanwhile, the electrolyte employed in each cell was decreased to 20 μL, resulting in a relatively lean electrolyte condition, ≈10.6 mL Ah^{-1}. The evolution of specific capacity and CE of such cells upon cycling is summarized in Figure 3c. The dis-/charge profiles of the cells with FE or FEmF of selected cycles are shown in Figure S12 (Supporting Information) and Figure 3d, respectively. When FE is employed, a continuous capacity fading is observed leading to a capacity retention of 17% after 250 cycles, which can be attributed to the limited Li inventory, i.e., thin LMA, in the cell. In contrast, the capacity retention of the Li/FEmF/SPAN cell after 250 cycles is 71%, resulting from the superior reversibility of both LMA and SPAN in FEmF. The specific energy based on the weight of SPAN and lithium metal in the Li/FEmF/SPAN cell is calculated to be 832 Wh kg^{-1} at 0.1 C and 750 Wh kg^{-1} at the elevated current rate (Figure S13, Supporting Information).

2.4. Chemistry at Electrode/electrolyte Interphases

The electrochemical results clearly demonstrate the high compatibility of SPAN cathodes with both FE and FEmF electrolytes, and the positive effect of mFBn co-solvent on the cyclability of LMAs. The cathodic LSV profiles of FE and FEmF indicate the influence of mFBn on the cathodic reduction of the electrolytes (Figure S14, Supporting Information), implying that the EEI

generated in these two electrolytes is different. Therefore, the EEIs formed on LMAs and SPAN cathodes recovered from the Li (500 µm)/SPAN cells after 103 cycles were investigated.

The surface morphology of pristine and cycled (in either FE or FEmF) SPAN electrodes was firstly examined via SEM (Figure S15, Supporting Information). Essentially, the images do not show distinguishable differences. Then, X-ray photoelectron spectroscopy (XPS) was employed to investigate the elemental composition and chemistry of the electrodes' surface layer (see **Figure 4**).

In the C 1s spectra of the pristine electrode (Figure 4a), the peak at 284.8 eV is assigned to C–C/C=C bonds of SPAN and carbon black additive.[52–54] The C–N group of SPAN together with the C–O groups of the binder gives rise to the peak at 286.3 eV.[52–54] The peak at 288.8 eV is attributed to C=O species from the binder.[54] After cycling, the peak attributed to C–N/C–O species shifts to 286.6 eV, which implies a different chemistry on the electrode's surface, namely a larger contribution of C–O species.

The spectra in the S 2p region show a multitude of sulfur species. For the pristine electrode, the S $2p_{3/2}$ peaks at 161.8,

163.8, 166.9, and 168.6 eV are assigned to HS_xC species, S–S, sulfite, and sulfate in SPAN, respectively.[52] It should be mentioned that the Se 3p peak doublet also appears in this region (Se $3p_{3/2}$ at ≈162 eV and Se $3p_{1/2}$ at ≈168 eV for elemental Se); however, comparison to the peak intensity in the Se 3d region (Figure S16, Supporting Information) indicates that the Se 3p peak intensity should be rather negligible.[55,56] For the electrodes cycled in either FE (Figure 4b) or FEmF (Figure 4c), the intensity of the S–S and HS_xC features is significantly reduced, while the intensity of sulfite increases. Furthermore, a new peak doublet is identified at higher binding energy (170.0 eV for S $2p_{3/2}$), which can be attributed to the FSI^- anion.[56,57] The ≈100% capacity retention of Li/SPAN cells in the initial 100 dis-/charge cycles excludes severe loss of sulfur from the SPAN cathodes. Therefore, the changes occurring in the S 2p spectra of cycled electrodes are certainly associated with the formation of a CEI on the SPAN cathodes. Furthermore, considering the much lower intensity of the peaks associated to SPAN than those of the CEI, one could further infer that the observed XPS signals from the cycled SPAN cathodes mainly originate from the CEIs. The presence of a CEI on the cycled SPAN
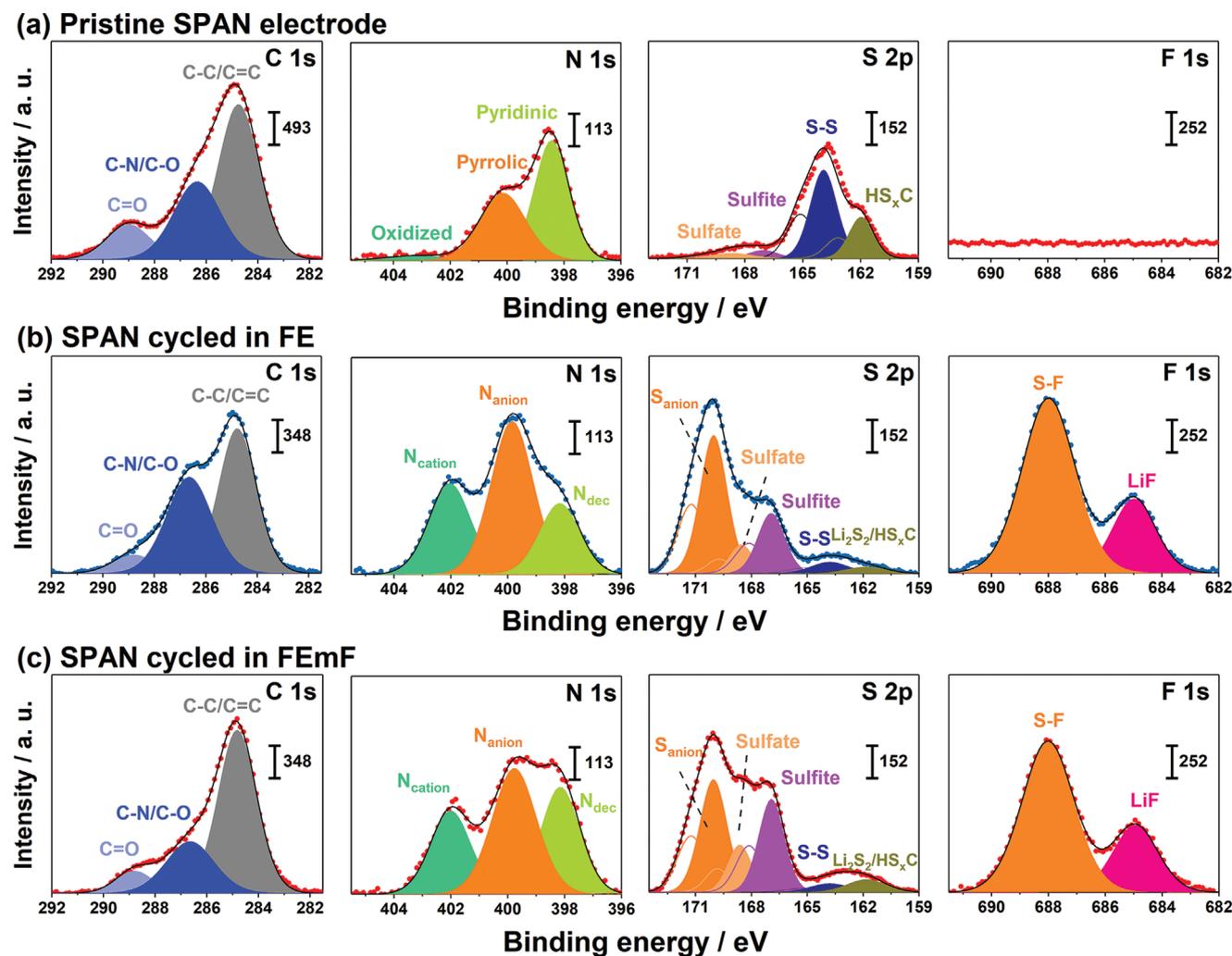

Figure 4. a–c) XPS detail spectra in the C 1s, N 1s, S 2p, and F 1s regions for SPAN cathodes at the pristine state (a), and after 103 cycles in FE (b) and FEmF (c) (after background subtraction).

electrodes is also corroborated by the F 1s spectra. While no fluorine signal could be detected for the pristine SPAN electrode, peaks of S–F (from FSI^-) and LiF were observed ≈688.0 and 685.0 eV, respectively, for the cycled SPAN cathodes.[30,58] These two species, particularly LiF that can only be generated by the electrolyte decomposition, unequivocally prove the presence of CEIs on the cycled SPAN electrodes. In the N 1s spectra of the pristine electrode, three peaks at 398.2, 399.9, and 403.1 eV were observed, which can be assigned to pyridinic, pyrrolic, and oxidized nitrogen in SPAN, respectively.[52] After cycling, three peaks due to the different nitrogen-containing species in the CEIs were detected. The peaks at 401.9 and 399.8 eV represent the positively charged nitrogen atoms (N_{cation}) from $Emim^+$ and negatively charged nitrogen atoms (N_{anion}) from FSI^-, respectively.[59] The peak at 398.1 eV (N_{dec}) can be attributed to nitrogen-containing species formed upon incomplete decomposition of $Emim^+$ and FSI^-, e.g., $LiN_xC_yH_z$ from $Emim^+$ and $LiNS_xO_yF_z$ from FSI^-.[60,61]

Since the C–C/C=C (C 1s), S–F (F 1s), and LiF (F 1s) peaks in both cycled samples exhibit very similar binding energy and intensity, the contribution of mFBn decomposition to the CEI appears to be limited. Therefore, the CEIs on SPAN are mainly generated from the deposition/decomposition of FSI^- and $Emim^+$. This also explains the generally similar composition of the CEIs formed in FE and FEmF. Even though, certain differences in the concentration of some species could still be observed. For example, compared with that for the FE sample, N_{dec} (N 1s), sulfate (S 2p), and sulfite (S 2p) showed higher intensity while N_{anion} (N 1s) and S_{anion} (S 2p) exhibited lower intensity for the FEmF sample. This difference reveals that the presence of mFBn leads to a slightly more extensive decomposition of FSI^-.

The SEM images of LMAs after cycling in Li/SPAN cells are shown in **Figure 5**a–d. The electrode cycled in FE appears to have a rougher, i.e., more porous, surface than that cycled in FEmF. The rougher surface morphology increases the contact area with the electrolyte, which could accelerate the side reactions at the interface. According to the SEM cross-sectional images (Figure 5b,d), the thickness of the corrosion layer in FE and FEmF is 65 and 22 µm, respectively, which clearly verifies more severe degradation of LMAs in FE. These results are identical to the electrochemical properties of Li/Cu, Li/Li, and Li/SPAN cells.

The XPS spectra of the LMAs cycled in FE and FEmF are shown in Figure 5e,f, respectively. In general, the components
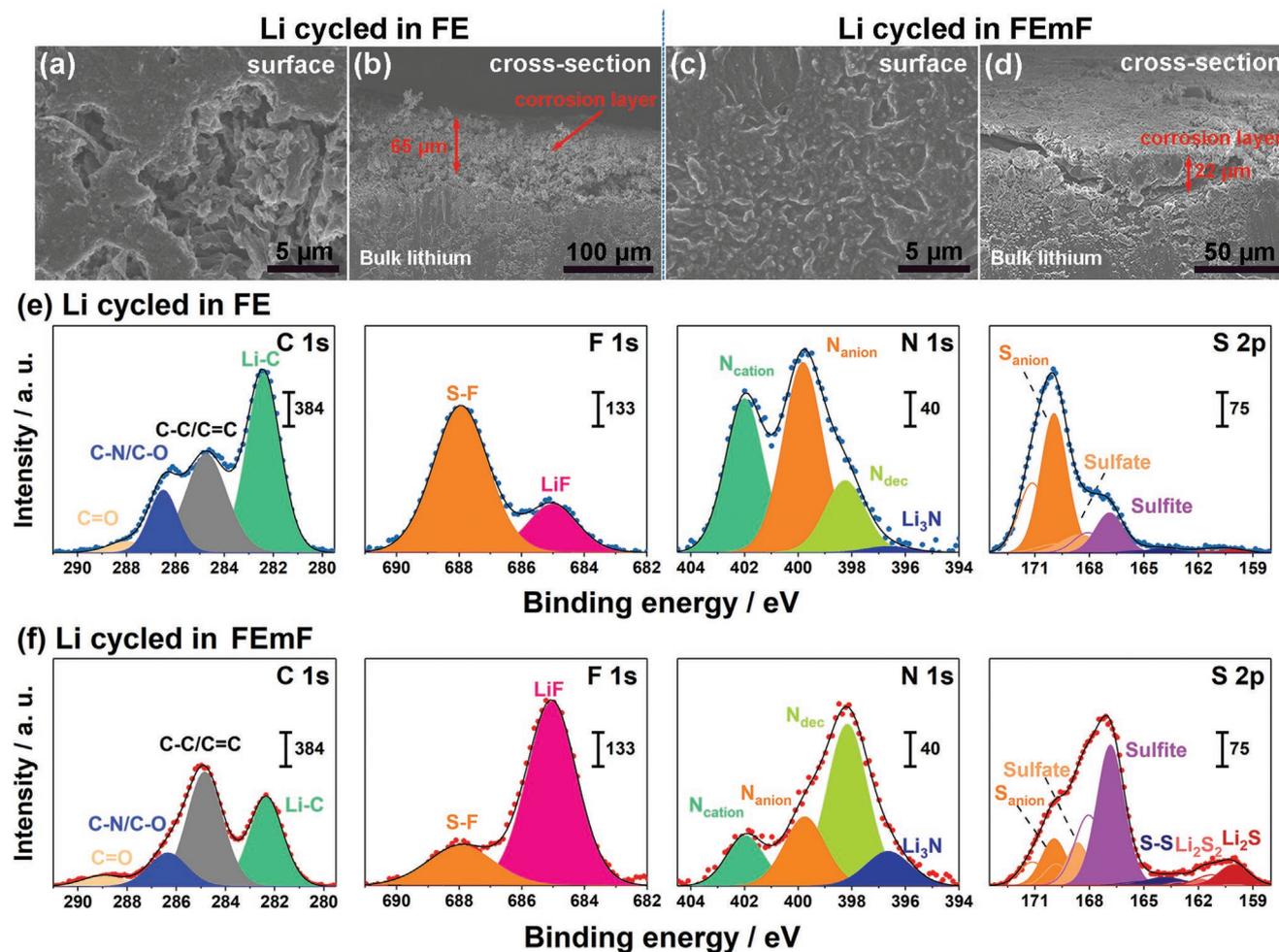

Figure 5. Characterization of LMAs unmounted from Li/SPAN cells after 103 cycles. a–d) SEM images of LMAs cycled in FE (a,b) and FEmF (c,d). e,f) XPS detail spectra in the C 1s, F 1s, N 1s, and S 2p regions for LMAs cycled in FE (e) and FEmF (f) (after background subtraction).

of the SEIs formed in the two electrolytes are similar. Most of the species making up the CEI on SPAN cathodes are also observed in the SEIs on LMAs, which is expected as these species are generated via the decomposition of the same compounds, i.e., $Emim^+$, FSI^-, and mFBn. Meanwhile, two new components are observed at 282.4 eV in C 1s spectra and 396.7 eV in N 1s spectra of LMAs, corresponding to Li–C species from the decomposition of $Emim^+$ and Li_3N species from the completed decomposition of $Emim^+$ or/and FSI^-, respectively.[60,62] Their presence demonstrates a deeper decomposition of $Emim^+$ and FSI^- on LMAs than on SPAN, which is caused by the lower potential, i.e., more reductive, of LMAs.

A more detailed comparison of Figure 5e,f reveals that the concentration of the SEI components highly depends on the electrolyte. The peaks of Li–C (C 1s), C–N/C–O (C 1s), and N_{cation} (N 1s) are more intense in Figure 5e, which demonstrates the less deep decomposition of $Emim^+$ in FEmF than in FE. As evidenced by the lower intensity of the S–F (F 1s), N_{anion} (N 1s), and S_{anion} (S 2p) peaks in Figure 5f, the SEI formed in FEmF also exhibits lower contents of FSI^- than that formed in FE. Nonetheless, a higher concentration of the species generated via the decomposition of FSI^-, e.g., sulfate, sulfite, Li_2S_2, and Li_2S, is observed in the S 2p spectra of the LMA cycled in FEmF. Therefore, the presence of mFBn in the electrolyte leads to deeper decomposition of FSI^-, which also contributes to the increased concentration of LiF (F 1s), N_{dec} (N 1s), and Li_3N (N 1s) in the LMA cycled in FEmF. It has been demonstrated that the inorganic species, e.g., LiF, Li_3N, etc., which exhibit high interfacial energy with lithium metal and high mechanical strength, are desirable components for robust SEIs suppressing dendritic growth and interfacial side reactions.[58,61,63] Therefore, their higher concentration in the SEI of the LMA cycled in FEmF is beneficial for the overall electrochemical performance.

3. Conclusion

A low-flammability LCILE employing partially solvating mFBn as the co-solvent has been developed for Li/SPAN cells. CEIs derived mainly from the decomposition of $Emim^+$ and FSI^- are generated on the SPAN electrodes upon cycling in either FE or FEmF, preventing the dissolution of polysulfides. The addition of mFBn to FE triggers a deeper decomposition of FSI^-, which in turn leads to the formation of an inorganic-rich SEI and highly reversible, dendrite-free LMAs. Benefiting from the stable EEIs simultaneously formed on both LMAs and SPAN cathodes in FEmF, highly stable cycling of Li/SPAN cells even with a very low excess of lithium has been achieved.

Supporting Information

Supporting Information is available from the Wiley Online Library or from the author.

Acknowledgements

Conflict of Interest

The authors declare no conflict of interest.

Authors Contribution

X.L.: Conceptualization, Electrochemical tests, Writing-original draft. T.D.: XPS measurements, Writing-review & editing. A.Ma..: MD simulation, Writing-review & editing. M.E.D.P.: NMR measurements, Writing-review & editing. X.D.: Tests for physicochemical properties, Writing-review & editing. A.Me.: NMR measurements, Writing-review & editing. S.P.: Supervision, Funding acquisition, Writing-review & editing.

Data Availability Statement

The data that support the findings of this study are available on request from the corresponding author. The data are not publicly available due to privacy or ethical restrictions.

Keywords

[1] X. Ji, K. T. Lee, L. F. Nazar, *Nat. Mater.* **2009**, *8*, 500.

[2] L. Wang, Y. Ye, N. Chen, Y. Huang, L. Li, F. Wu, R. Chen, *Adv. Funct. Mater.* **2018**, *28*, 1800919.

[3] W. P. Wang, J. Zhang, J. Chou, Y. X. Yin, Y. You, S. Xin, Y. G. Guo, *Adv. Energy Mater.* **2020**, *11*, 2000791.

[4] J. Wang, J. Yang, J. Xie, N. Xu, *Adv. Mater.* **2002**, *14*, 963.

[5] M. S. Ahmed, S. Lee, M. Agostini, M. G. Jeong, H.-G. Jung, J. Ming, Y.-K. Sun, J. Kim, J.-Y. Hwang, *Adv. Sci.* **2021**, *8*, 2101123.

[6] H. Yang, J. Chen, J. Yang, J. Wang, *Angew. Chem., Int. Ed.* **2020**, *59*, 7306.

[7] J. Chen, H. Lu, X. Zhang, Y. Zhang, J. Yang, Y. Nuli, Y. Huang, J. Wang, *Energy Storage Mater.* **2022**, *50*, 387.

[8] B. He, Z. Rao, Z. Cheng, D. Liu, D. He, J. Chen, Z. Miao, L. Yuan, Z. Li, Y. Huang, *Adv. Energy Mater.* **2021**, *11*, 2003690.

[9] Z. Shen, W. Zhang, S. Mao, S. Li, X. Wang, Y. Lu, *ACS Energy Lett.* **2021**, *6*, 2673.

[10] W. Wang, Z. Cao, G. A. Elia, Y. Wu, W. Wahyudi, E. Abou-Hamad, A. H. Emwas, L. Cavallo, L.-J. Li, J. Ming, *ACS Energy Lett.* **2018**, *3*, 2899.

[11] Z. Wu, S.-M. Bak, Z. Shadike, S. Yu, E. Hu, X. Xing, Y. Du, X.-Q. Yang, H. Liu, P. Liu, *ACS Appl. Mater. Interfaces* **2021**, *13*, 31733.

[12] X. Liu, M. Zarrabeitia, A. Mariani, X. Gao, H. M. Schütz, S. Fang, T. Bizien, G. A. Elia, S. Passerini, *Small Methods* **2021**, *5*, 2100168.

[13] H. Wang, Z. Yu, X. Kong, S. C. Kim, D. T. Boyle, J. Qin, Z. Bao, Y. Cui, *Joule* **2022**, *6*, 588.

[14] G. Xu, L. Huang, C. Lu, X. Zhou, G. Cui, *Energy Storage Mater.* **2020**, *31*, 72.

[15] J. Xiao, Q. Li, Y. Bi, M. Cai, B. Dunn, T. Glossmann, J. Liu, T. Osaka, R. Sugiura, B. Wu, J. Yang, J.-G. Zhang, M. S. Whittingham, *Nat. Energy* **2020**, *5*, 561.

[16] W.-J. Chen, B.-Q. Li, C.-X. Zhao, M. Zhao, T.-Q. Yuan, R.-C. Sun, J.-Q. Huang, Q. Zhang, *Angew. Chem., Int. Ed.* **2020**, *59*, 10732.

[17] H. Liu, J. Holoubek, H. Zhou, A. Chen, N. Chang, Z. Wu, S. Yu, Q. Yan, X. Xing, Y. Li, T. A. Pascal, P. Liu, *Mater. Today* **2021**, *42*, 17.

[18] H. Yang, Y. Qiao, Z. Chang, P. He, H. Zhou, *Angew. Chem., Int. Ed.* **2021**, *60*, 17726.

[19] Y. He, P. Zou, S.-M. Bak, C. Wang, R. Zhang, L. Yao, Y. Du, E. Hu, R. Lin, H. L. Xin, *ACS Energy Lett.* **2022**, *7*, 2866.

[20] M. Hasanpoor, D. Saurel, R. C. Barreno, K. Fraysse, M. Echeverría, M. Jáuregui, F. Bonilla, G. W. Greene, R. Kerr, M. Forsyth, P. C. Howlett, *ACS Appl. Mater. Interfaces* **2022**, *14*, 13196.

[21] F. Wu, S. Fang, M. Kuenzel, A. Mullaliu, J.-K. Kim, X. Gao, T. Diemant, G.-T. Kim, S. Passerini, *Joule* **2021**, *5*, 2177.

[22] U. Pal, D. Rakov, B. Lu, B. Sayahpour, F. Chen, B. Roy, D. R. MacFarlane, M. Armand, P. C. Howlett, Y. S. Meng, M. Forsyth, *Energy Environ. Sci.* **2022**, *15*, 1907.

[23] X. Liu, A. Mariani, M. Zarrabeitia, M. E. Di Pietro, X. Dong, G. A. Elia, A. Mele, S. Passerini, *Energy Storage Mater.* **2022**, *44*, 370.

[24] Z. Wang, F. Zhang, Y. Sun, L. Zheng, Y. Shen, D. Fu, W. Li, A. Pan, L. Wang, J. Xu, J. Hu, X. Wu, *Adv. Energy Mater.* **2021**, *11*, 2003752.

[25] S. Lee, K. Park, B. Koo, C. Park, M. Jang, H. Lee, H. Lee, *Adv. Funct. Mater.* **2020**, *30*, 2003132.

[26] G. Zhang, X. Deng, J. Li, J. Wang, G. Shi, Y. Yang, J. Chang, K. Yu, S.-S. Chi, H. Wang, P. Wang, Z. Liu, Y. Gao, Z. Zheng, Y. Deng, C. Wang, *Nano Energy* **2022**, *95*, 107014.

[27] X. Cao, H. Jia, W. Xu, J.-G. Zhang, *J. Electrochem. Soc.* **2021**, *168*, 010522.

[28] C. Zhu, C. Sun, R. Li, S. Weng, L. Fan, X. Wang, L. Chen, M. Noked, X. Fan, *ACS Energy Lett.* **2022**, *7*, 1338.

[29] Z. Jiang, Z. Zeng, X. Liang, L. Yang, W. Hu, C. Zhang, Z. Han, J. Feng, J. Xie, *Adv. Funct. Mater.* **2021**, *31*, 2005991.

[30] D.-J. Yoo, S. Yang, K. J. Kim, J. W. Choi, *Angew. Chem., Int. Ed.* **2020**, *59*, 14869.

[31] X. Liu, A. Mariani, T. Diemant, M. E. Di Pietro, X. Dong, M. Kuenzel, A. Mele, S. Passerini, *Adv. Energy Mater.* **2022**, *12*, 2200862.

[32] American Occupational Safety and Health Standards, from https://www.osha.gov/laws-regs/regulations/standard-number/1910/1910.106 (accessed: August 2022).

[33] L. Tan, S. Chen, Y. Chen, J. Fan, D. Ruan, Q. Nian, L. Chen, S. Jiao, X. Ren, *Angew. Chem., Int. Ed.* **2022**, *61*, e202203693.

[34] R. S. Kühnel, N. Böckenfeld, S. Passerini, M. Winter, A. Balducci, *Electrochim. Acta* **2011**, *56*, 4092.

[35] C. Wohlfarth, *Phys. Chem.* **2017**, *2*, 206.

[36] J. Wang, Y. Yamada, K. Sodeyama, C. H. Chiang, Y. Tateyama, A. Yamada, *Nat. Commun.* **2016**, *7*, 12032.

[37] Y. Yamada, M. Yaegashi, T. Abe, A. Yamada, *Chem. Commun.* **2013**, *49*, 11194.

[38] M. Beran, J. Příhoda, Z. Žák, M. Černík, *Polyhedron* **2006**, *25*, 1292.

[39] G. Fogarasi, A. G. Császár, *Spectrochim. Acta, Part A* **1988**, *44*, 1067.

[40] S. Singh, D. K. Singh, S. K. Srivastava, B. P. Asthana, *Vib. Spectrosc.* **2011**, *56*, 26.

[41] N. E. Heimer, R. E. Del Sesto, Z. Meng, J. S. Wilkes, W. R. Carper, *J. Mol. Liq.* **2006**, *124*, 84.

[42] Y. Yamada, A. Yamada, *J. Electrochem. Soc.* **2015**, *162*, A2406.

[43] Y. Yamada, J. Wang, S. Ko, E. Watanabe, A. Yamada, *Nat. Energy* **2019**, *4*, 269.

[44] J.-G. Zhang, W. Xu, J. Xiao, X. Cao, J. Liu, *Chem. Rev.* **2020**, *120*, 13312.

[45] B. D. Adams, J. Zheng, X. Ren, W. Xu, J.-G. Zhang, *Adv. Energy Mater.* **2018**, *8*, 1702097.

[46] Y. Zhang, Y. Sun, L. Peng, J. Yang, H. Jia, Z. Zhang, B. Shan, J. Xie, *Energy Storage Mater.* **2019**, *21*, 287.

[47] M. Jiang, K. Wang, S. Gao, R. Wang, J. Han, J. Yan, S. Cheng, K. Jiang, *ChemElectroChem* **2019**, *6*, 1365.

[48] L. Wang, X. Chen, S. Li, J. Yang, Y. Sun, L. Peng, B. Shan, J. Xie, *J. Mater. Chem. A* **2019**, *7*, 12732.

[49] X. Chen, L. Peng, L. Wang, J. Yang, Z. Hao, J. Xiang, S. Yuan, Y. Huang, B. Shan, L. Yuan, J. Xie, *Nat. Commun.* **2019**, *10*, 1021.

[50] S. Li, W. Zhang, Z. Zeng, S. Cheng, J. Xie, *Electrochem. Energy Rev.* **2020**, *3*, 613.

[51] S. P. Beltran, P. B. Balbuena, *ACS Appl. Mater. Interfaces* **2021**, *13*, 491.

[52] C.-J. Huang, K.-Y. Lin, Y.-C. Hsieh, W.-N. Su, C.-H. Wang, G. Brunklaus, M. Winter, J.-C. Jiang, B. J. Hwang, *ACS Appl. Mater. Interfaces* **2021**, *13*, 14230.

[53] P. Louette, F. Bodino, J.-J. Pireaux, *Surf. Sci. Spectra* **2005**, *12*, 22.

[54] M. Hekmatfar, A. Kazzazi, G. G. Eshetu, I. Hasa, S. Passerini, *ACS Appl. Mater. Interfaces* **2019**, *11*, 43166.

[55] V. H. Pham, J. A. Boscoboinik, D. J. Stacchiola, E. C. Self, P. Manikandan, S. Nagarajan, Y. Wang, V. G. Pol, J. Nanda, E. Paek, D. Mitlin, *Energy Storage Mater.* **2019**, *20*, 71.

[56] J. F. Moulder, W. F. Stickle, P. E. Sobol, K. D. Bomben, Handbook of X-Ray Photoelectron Spectroscopy, Physical Electronics Division, Perkin-Elmer Corp, Eden Prairie, MN, USA **1995**.

[57] G. G. Eshetu, T. Diemant, M. Hekmatfar, S. Grugeon, R. J. Behm, S. Laruelle, M. Armand, S. Passerini, *Nano Energy* **2019**, *55*, 327.

[58] X. Fan, L. Chen, X. Ji, T. Deng, S. Hou, J. Chen, J. Zheng, F. Wang, J. Jiang, K. Xu, C. Wang, *Chem* **2018**, *4*, 174.

[59] M. Olschewski, R. Gustus, O. Höfft, A. Lahiri, F. Endres, *J. Phys. Chem. C* **2017**, *121*, 2675.

[60] M. Olschewski, R. Gustus, M. Marschewski, O. Höfft, F. Endres, *Phys. Chem. Chem. Phys.* **2014**, *16*, 25969.

[61] S. Liu, X. Ji, N. Piao, J. Chen, N. Eidson, J. Xu, P. Wang, L. Chen, J. Zhang, T. Deng, S. Hou, T. Jin, H. Wan, J. Li, J. Tu, C. Wang, *Angew. Chem., Int. Ed.* **2021**, *60*, 3661.

[62] K. Park, B.-C. Yu, J. B. Goodenough, *Adv. Energy Mater.* **2016**, *6*, 1502534.

[63] X. Ren, S. Chen, H. Lee, D. Mei, M. H. Engelhard, S. D. Burton, W. Zhao, J. Zheng, Q. Li, M. S. Ding, M. Schroeder, J. Alvarado, K. Xu, Y. S. Meng, J. Liu, J.-G. Zhang, W. Xu, *Chem* **2018**, *4*, 1877.